



Research Article

ISSN : 0975-7384
CODEN(USA) : JCPRC5

Electrochemical, SEM/EDX study of 3-Ethyl-4-amino-5-mercapto-1,2,4-triazole as inhibitor for corrosion of 6061 Al-15 vol. Pct. SiC(p) composite and its base alloy in sulphuric acid medium

Geetha Mable Pinto^{*}, Ronald Nazareth^a, A. Nityananda Shetty^b and Jagannath Nayak^c

^{*}Department of Chemistry, St. Agnes College, Mangaluru- 575002, Karnataka, India

^aDepartment of Chemistry, St. Aloysius College, Mangaluru- 575003, Karnataka, India

^bDepartment of Chemistry, National Institute of Technology Karnataka, Surathkal, Srinivasnagar-575 025, Karnataka, India

^cDepartment of Metallurgical and Materials Engineering, National Institute of Technology Karnataka, Surathkal, Srinivasnagar-575 025, Karnataka, India

ABSTRACT

The inhibitive action of 3-Ethyl-4-amino-5-mercapto-1, 2, 4-triazole on the corrosion behavior of 6061 Al -15 vol. pct. SiC(p) composite and its base alloy was studied at different temperatures in sulphuric acid medium containing varying concentrations of it, using Tafel extrapolation technique and AC impedance spectroscopy (EIS). Results showed that EAMT was an effective inhibitor, showing inhibition efficiency of 85% in 0.5 M sulfuric acid. The adsorption of EAMT on both the composite and base alloy was found to be through chemisorption obeying Langmuir adsorption isotherm. The thermodynamic parameters such as free energy, enthalpy and entropy of adsorption, and activation parameters were calculated.

Key words: Alloys, Electrochemical techniques, Adsorption, Corrosion

INTRODUCTION

Aluminium matrix composites (AMCs) have received considerable attention for military, automobile and aerospace applications because of their low density, high strength and high stiffness [1- 5]. Further the addition of ceramic reinforcements (SiC) has raised the performance limits of the Al (6061) alloys [6]. It is known that aluminium matrix composites exhibited better resistance to mechanical wear than their base alloys and hence they have specific strength for numerous weight sensitive applications [7,8]. One of the main disadvantages in the use of metal matrix composite is the influence of reinforcement on corrosion rate. The addition of a reinforcing phase could lead to discontinuities in the film, thereby increasing the number of sites where corrosion can be initiated and making the composites more susceptible for corrosion [7,9]. However the high corrosion rates of these composites, particularly in acid media can be combated using inhibitors [10,11]. Due to the wide applications of such composites, they frequently come in contact with acid during cleaning, pickling, descaling, etc. A wide variety of compounds are used as inhibitors in acid media. These are mainly organic compounds containing N, S or O atoms [10-14] and critical use of these compounds in industries has also been reviewed [15-17]. Owing to their usefulness in several stages of process industries, organic compounds containing both N and S atoms function as better adsorption inhibitors because of their lone pair of electrons and polar nature of the molecules [18]. Inhibitive action of EAMT on the

corrosion behavior of Al-SiC composites in 0.125 M - 0.5 M H₂SO₄ solution at four levels of concentrations of the inhibitor at five different temperatures are carried out.

EXPERIMENTAL SECTION

2.1. Material

The experiments were performed with specimens of 6061 Al-15 vol.pct. SiC(p) composite and its base alloy in extruded rod form (extrusion ratio 30:1). The composition of the base metal 6061 Al alloy is given in Table 1. Cylindrical test coupons were cut from the rods and sealed with epoxy resin in such a way that, the areas of the composite and the base alloy, exposed to the medium were 0.95 cm² and 0.785 cm², respectively. These coupons were polished as per standard metallographic practice, belt grinding followed by polishing on emery papers, and finally on polishing wheel using levigated alumina to obtain mirror finish. It was then degreased with acetone, washed with double distilled water and dried before immersing in the corrosion medium.

2.2. Medium

Standard solution of sulphuric acid was prepared from analytical grade (Nice) acids. The three solutions used for the study were with the following concentrations of sulphuric acid respectively: 0.5 M, 0.25 M and 0.125 M. Experiments were carried out using calibrated thermostat at temperatures 30 °C, 35 °C, 40 °C, 45 °C, 50 °C (±0.5 °C). Inhibitive action of EAMT on the corrosion behavior of Al-SiC composites in 0.125 M - 0.5 M H₂SO₄ solution at four levels of concentrations of the inhibitor at five different temperatures are carried out.

2.3. Electrochemical measurements

2.3.1. Tafel polarization studies

Electrochemical measurements were carried out by using an electrochemical work station, Auto Lab 30 and GPES software. Tafel plot measurements were carried out using conventional three electrode Pyrex glass cell with platinum counter electrode and saturated calomel electrode (SCE) as reference electrode. All the values of potential are therefore referred to the SCE. Finely polished composite and base alloy specimens were exposed to corrosion medium of different concentrations of sulphuric acid at different temperatures (30 °C to 50 °C) and allowed to establish a steady state open circuit potential. The potentiodynamic current-potential curves were recorded by polarizing the specimen to -250 mV cathodically and +250 mV anodically with respect to open circuit potential (OCP) at scan rate of 1 mV s⁻¹.

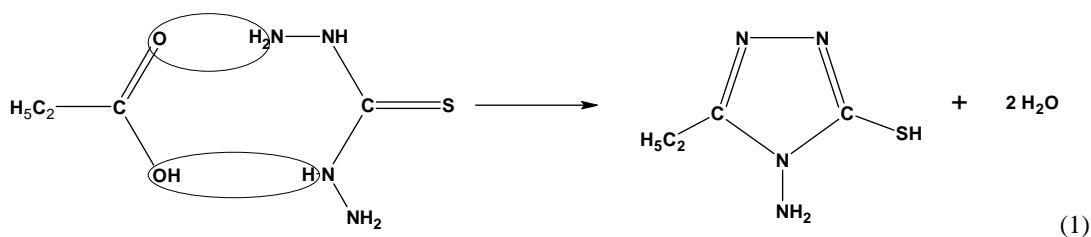
2.3.2. Electrochemical impedance spectroscopy studies (EIS)

The corrosion behaviors of the specimens of the composite and the base alloy were also obtained from EIS technique using electrochemical work station, Auto Lab 30 and FRA software. In EIS technique a small amplitude ac signal of 10 mV and frequency spectrum from 100 kHz to 0.01 Hz was impressed at the OCP and impedance data were analyzed using Nyquist plots. The charge transfer resistance, R_t was extracted from the diameter of the semicircle in Nyquist plot.

In all the above measurements, at least three similar results were considered and their average values are reported.

2.4. Synthesis of 3 - Ethyl - 4 - amino -5 - mercapto -1, 2, 4 - triazole

3 - Ethyl - 4 - amino -5 - mercapto -1, 2, 4 - triazole was synthesized and recrystallised as per the reported procedure [19]. A mixture of thiocarbohydrazide (10g) and propionic acid (60 ml) was heated, under reflux on wire gauze for 4 hours. The product was recrystallised from ethanol. Colourless shining crystals were obtained. The recrystallised product was checked by IR, elemental analysis and melting point.



2.5. Scanning electron microscopy (SEM) analysis

Imaging was done on an FEI Quanta 400 ESEM in the Hi-Vac mode, without any gold coating, 30kV accelerating voltage and appropriate spot sizes of the beam (3.5). The stubs were placed in the specimen chamber stage using double-sided graphite coated tape in order to reduce/remove any sample drift. The EDX spectra of the samples were recorded using JEOL JSM – 6380 LA analytical scanning electron microscope.

RESULTS AND DISCUSSION

3.1. Potentiodynamic polarization (PDP) measurements

The polarization studies of aluminum specimens were carried out in 0.125 M – 0.5 M sulphuric acid solutions separately in absence and presence of different concentrations of EAMT. Fig. 1 and Fig. 2 represents potentiodynamic polarization curve of 6061 Al – SiC composite and its base alloy at various concentrations of EAMT in 0.5 M sulphuric acid at 30 °C solutions in the absence and presence of EAMT. Similar results were obtained in the same concentrations of acid medium at four other temperatures and also in the other two concentrations of the sulphuric acid at the five temperatures studied. The following conclusions can be drawn from the figures.

The potentiodynamic polarization parameters like corrosion potential (E_{corr}), corrosion currents (I_{corr}) and cathodic slopes (b_c) are calculated from Tafel plots for both the composite and base alloy. The data in the Table 2 clearly show that the addition of EAMT decreases the corrosion rates of both the composite and the base alloy. Inhibition efficiency increases with increasing EAMT concentration. For the inhibited systems, the values of E_{corr} are shifted to more negative direction and leftward displacement in the cathodic branch of the curves. According to [20 -22] these are typical features of cathodic inhibitors, this being in agreement with the results obtained for other aluminum alloys.

Since the linear portion at the anodic region is not well defined, the corrosion current densities are determined by the extrapolation of cathodic Tafel slopes to the respective corrosion potentials. The Tafel slopes remain almost unchanged for the uninhibited and inhibited systems, indicated that the inhibitive action of EAMT occurred by simple blocking of the available area. In other words, the inhibitors decreased the surface area available for anodic dissolution and hydrogen evolution without affecting the reaction mechanism and only causes inactivation of part of the surface [23, 24]. This fact is an important observation, since the presence of SiC particles in the composite initiates cathodic sites which is responsible for the higher corrosion of the composite than that of the base alloy [7, 9]. Therefore blocking of these sites via EAMT adsorption would result in decreasing the corrosion rate of composite to a greater extent as compared to the base alloy. The comparison of inhibition efficiency of EAMT for the composite and base alloy at different concentrations and different temperatures shows that the inhibition effect is more on the composite than on the base alloy. The increase in the efficiency of the inhibitor in the case of composite may be due to its heterogenic nature, where the incorporation of silicon carbide acts as the potential active site for the adsorption of the inhibitor. The increase in inhibition efficiency with increasing inhibitor concentration indicates that more inhibitor molecules are adsorbed on the metal surface, thus providing wider surface coverage.

The electrochemical parameters (E_{corr} , i_{corr} , b_a and b_c) associated with the polarization measurements at different EAMT concentrations as well as at different temperatures for the composite and the base alloy in 0.5 M sulphuric acid media are listed in Table 2.

$$\theta = \frac{i_{\text{corr}}(\text{uninh}) - i_{\text{corr}}(\text{inh})}{i_{\text{corr}}(\text{uninh})} \quad (2)$$

Inhibition efficiency can be calculated

$$\text{IE} (\%) = \theta \times 100 \quad (3)$$

3.2. Electrochemical impedance spectroscopy (EIS) measurements

Corrosion behavior of 6061 Al- SiC composite and its base alloy were carried out in 0.125 M– 0.5 M H_2SO_4 solutions separately in absence and presence of different concentrations of EAMT. Fig. 3 and Fig. 4 represents

Nyquist plots of 6061 Al – SiC composite and its base alloy at various concentrations of EAMT in 0.5 M H₂SO₄ at 30 °C respectively.

As can be seen from the Fig. 3 and Fig 4, the impedance diagrams show semicircles, indicating that the corrosion process is mainly charge transfer controlled. It is also clear from the figures that the shapes of the impedance plots for inhibited specimens are not different from those of uninhibited one. The presence of inhibitor increases the impedance but doesn't change other aspects of the behavior. These results support the results of potentiodynamic polarization measurements that the inhibitor does not alter the mechanism of electrochemical reactions responsible for corrosion. In the Nyquist plots for the 6061Al-SiC composite, the impedance spectra consists of a large capacitive loop at high frequencies (HF) and an inductive loop at low frequencies (LF). Similar impedance plots have been reported in literature for the corrosion of pure aluminium and aluminium alloys in various electrolytes such as sodium sulphate [25 -27], sulphuric acid [26, 27] acetic acid [26], sodium chloride [28 , 29] and hydrochloric acid [24, 30 – 35]. The general shape of the curve is similar for all individual samples of the base alloy, with large capacitive loop at high frequencies (HF) and an inductive loop at intermediate frequencies (IF), followed by a second capacitive loop at low frequency (LF) values. Similar results have been reported in literature for the corrosion of pure aluminum in acidic and neutral solutions [25, 26].

The high frequency capacitive loop could be assigned to the charge transfer of the corrosion process and to the formation of oxide layer [36, 37]. The oxide film is considered to be a parallel circuit of a resistor due to the ionic conduction in the oxide film and a capacitor due to its dielectric properties. According to Brett [31, 33], the capacitive loop is corresponding to the interfacial reactions, particularly, the reaction of aluminum oxidation at the metal/oxide/electrolyte interface. The process includes the formation of Al⁺ ions at the metal/oxide interface, and their migration through the oxide/solution interface where they are oxidized to Al³⁺. At the oxide/solution interface, OH⁻ or O²⁻ ions are also formed. The fact that all the three processes are represented by only one loop could be attributed either to the overlapping of the loops of processes, or to the assumption that one process dominates and, therefore, excludes the other processes [27] The other explanation offered to the high frequency capacitive loop is the oxide film itself. This was supported by a linear relationship between the inverse of the capacitance and the potential found by Bessone et. al and Wit and Lenderink [27, 28]

The origin of the inductive loop has often been attributed to surface or bulk relaxation of species in the oxide layer [29]. The LF inductive loop may be related to the relaxation process obtained by adsorption and incorporation of sulphate ions, oxygen ion and charged intermediates on and into the oxide film [26]. The second capacitive loop observed at LF values could be assigned to the metal dissolution [25]. The measured values of polarization resistance increase with the increasing concentration of EAMT in the solution, indicating decrease in the corrosion rate for the base metal with increase in EAMT concentration up to critical concentration of the inhibitor. This is in accordance with the observations obtained from potentiodynamic measurements.

However, in the case of Al/SiC composites, the obtained semicircles in absence or in presence of inhibitor were depressed. Deviation of this kind are referred to as frequency dispersion, have been attributed to inhomogeneties of solid surfaces, as the aluminum composite is reinforced with SiC particles. Mansfeld et al. [36, 37] have suggested an exponent n in the impedance function as a deviation parameter from the ideal behavior. By this suggestion, the capacitor in the equivalent circuit can be replaced by a so-called constant phase element (CPE) that is a frequency-dependent element and related to surface roughness. The impedance function of a CPE has the following equation [26]

$$Z_{\text{CPE}} = \frac{1}{(Y_0 j\omega)^n} \quad (4)$$

where the amplitude Y_0 and n are frequency independent, and ω is the angular frequency for which $-Z''$ reaches its maximum values, n is dependent on the surface morphology: $-1 \leq n \leq 1$. R_i and CPE have opposite trend at the whole concentration range. It can be supposed that a protective layer covers the surface of the electrode. The IE% values indicate that by the increase of inhibitor concentrations, their values increase too. The double layer between the charged metal surface and the solution is considered as an electrical capacitor. The adsorption of EAMT on the aluminum surface decreases its electrical capacity because they displace the water molecules and other ions originally adsorbed on the surface. The decrease in this capacity with increase in EAMT concentrations may be attributed to the formation of a protective layer on the electrode surface. The thickness of this protective layer

increases with increase in inhibitor concentration up to their critical concentration. The obtained CPE (Q) values decreases noticeably with increase in the concentration of EAMT up to their critical concentration. In the case of composites, adsorption of negatively charged heteroatoms and π electrons of the benzene ring of EAMT at the Al/SiC interface occurs to a better extent than the base alloy. (Q is inversely proportional to the thickness of the surface film or protective layer). In the case of base alloys due to the homogenous surface, frequency dispersion is very less. Therefore the obtained semicircles in the impedance spectra are less depressed. The increase in the efficiency of the inhibitor in the case of composite may be due to its heterogenic nature, where the incorporation of silicon carbide acts as the potential active site for the adsorption of the inhibitor.

The measured values of charge transfer resistance indicate that the rate of corrosion decreases with increase in concentration of inhibitor solution. Since R_t is inversely proportional to the corrosion current and it can be used to calculate the inhibition efficiency from the relation,

$$IE \% = \frac{\left[\frac{1}{R_t} \right]_0 - \left[\frac{1}{R_t} \right]}{\left[\frac{1}{R_t} \right]_0} \times 100 \quad (5)$$

where $[R_t]_0$ and $[R_t]$ are the charge transfer resistances in the presence and absence of inhibitors.

A comparison of the inhibiting efficiencies obtained using a.c. and d.c methods show that acceptable agreement is achieved. In the studied frequency range, the system could be described by two time constant model, as shown in Fig 5. An equivalent circuit of five elements depicted in Fig. 5 a was used to simulate the measured impedance data as shown in Fig. 5 b. In this equivalent circuit R_s is the solution resistance and R_t is the charge transfer resistance. R_L and L represent the inductive elements. This also consists of constant phase element, CPE (Q) in parallel to the parallel resistors R_t and R_L , and the later is in series with the inductor L. When an inductive loop is present, the polarization resistance R_p can be calculated from equation (6):

$$R_p = \frac{R_L \times R_t}{R_L + R_t} \quad (6)$$

An equivalent circuit of nine elements depicted in Fig. 6 a was used to simulate the measured impedance data of the base alloy as shown in Fig. 6 b. In this equivalent circuit R_s is the solution resistance and R_t is the charge transfer resistance. R_L and L represent the inductive elements. This also consists of constant phase element; CPE (Q) in parallel to the series capacitors C_1 , C_2 and series resistors R_1 , R_2 , R_L and R_t . R_L is parallel with the inductor L. When an inductive loop is present, the polarization resistance R_p and double layer capacitance C_{dl} can be calculated from equations (7) and (8):

$$R_p = R_L + R_t + R_1 + R_2 \quad (7)$$

$$C_{dl} = C_1 + C_2 \quad (8)$$

It can be seen that R_s (solution resistance) remain almost constant, with and without addition of EAMT for both the composite and its base alloy. It was also observed from Table 3 that the value of constant phase element, Q decreases, while the value of R_t increases with increasing concentration of EAMT up to their critical concentration, indicated that the inhibitor inhibits the corrosion of 6061 Al-SiC composite and base alloy by the adsorption mechanism [38].

The double layer between the charged metal surface and the solution is considered as an electrical capacitor. The adsorption of EAMT on the aluminum surface decreases its electrical capacity because they displace the water molecules and other ions originally adsorbed on the surface. The decrease in this capacity with increase in EAMT concentrations may be attributed to the formation of a protective layer on the electrode surface. The thickness of this protective layer increases with increase in inhibitor concentration up to their critical concentration and then

decreases. The obtained CPE (Q) values decrease with increase in the concentration of EAMT. Decrease in CPE, which can result from a decrease in local dielectric constant and/or an increase in the thickness of the electrical double layer, suggest that the inhibitor molecules act by adsorption at the metal/solution interface. The values of n obtained for EAMT inhibitor systems were close to unity which shows that the interface behaves nearly capacitive.

The Bode plots for 6061 Al/ SiC composite and its base alloy with and without inhibitor, obtained at OCP, are presented in Fig. 7 and Fig. 8. It is apparent that, in the case composite, the phase angle maxima are quite broad after addition of EAMT whereas there is no noticeable change observed for the base alloy.

3.3. Effect of the immersion time

Electrochemical impedance spectroscopy is a useful technique for long time tests, because they do not significantly disturb the system and it is possible to follow it overtime [56]. Immersion time experiments in the present work were carried out in various concentrations of acid mixture containing 400 ppm of inhibitor for 300 min and Nyquist plots were recorded every 10 min during the initial 40 min, and then every 30 min afterward. The results obtained (not shown here) showed that the immersion time has a great influence on the size and shape of the impedance spectra, and therefore the inhibition efficiency of the inhibitor. The capacitive loop was found to increase in size with the increase of immersion time, reaching a maximum in 40 min and remained fairly constant afterward. More details are shown in Fig. 9, which represents the variation of both R_i and CPE with the immersion time recorded for EAMT in 0.5 M sulphuric acid concentration at 30 °C. Similar results were obtained for other two concentrations of the sulphuric acid. It is obvious from Fig. 9, that the R_i values increased from 345 to 450 $\Omega \text{ cm}^2$ during the initial 40 min and remained fairly constant afterward. At the same time, the capacitance values were reduced drastically from 122 to 55 $\mu\text{F cm}^{-2}$ after 40 min and remained fairly constant afterward. This means that the formation of the inhibitor surface film, and therefore the inhibitor adsorption, on the electrode surface was fast and completed within 40 min. These results demonstrate that the inhibition efficiency increases with increasing immersion time. It is possible that with increasing immersion time and concentration, a compact adsorbed film of the inhibitor is formed on the aluminium surface, since adsorption of more EAMT is facilitated on the aluminium surface. The formation of such adsorbed film is confirmed by EDX examinations of the electrode surface.

3.4. Effect of temperature and activation parameters of inhibition process

It is observed that EAMT exhibits corrosion inhibiting property at all studied temperatures and the values of % IE for EAMT increase with increase in temperature. Table 4 gives the idea of change of electrochemical parameters with temperature obtained from PDP measurements of Al composite and its base alloy in 0.5 M H_2SO_4 in the absence and presence of various concentrations of EAMT.

Thus EAMT efficiencies were temperature dependent. Ivanov [39] considers the increase of % IE with increase of temperature as the change in the nature of the adsorption mode, the inhibitor is being physically adsorbed at lower temperatures, while chemisorption is favoured as temperature increases. Plot of $\ln(\text{corrosion rate})$ versus $1/T$ for 6061 Al composite and its base alloy in 0.5 M sulphuric acid in absence and presence of various concentrations of EAMT are shown in Fig. 10 and Fig. 11. As shown from these figures, straight lines were obtained according to Arrhenius – type equation:

$$\ln(\text{corrosion rate}) = A - \frac{E_a}{RT} \quad (9)$$

where K is the corrosion rate, A is constant depends on metal type and electrolyte, E_a is the apparent activation energy, R is the universal gas constant and T is the absolute temperature.

Plot of $\ln(\text{corrosion rate}/T)$ vs $1/T$ for both the samples of aluminium 6061 in 0.5 M sulphuric acid in absence and presence of various concentrations of EAMT is shown in Fig.12 and Fig.13. As shown from these Figures, straight lines were obtained according to transition state equation:

$$\text{Corrosion rate} = \frac{RT}{Nh} \frac{\Delta S^\ddagger}{eR} e^{-\frac{\Delta H^\ddagger}{RT}} \quad (10)$$

where h is Planck's constant, N is Avogadro's number, ΔH^\ddagger is the activation enthalpy and ΔS^\ddagger is the activation entropy. The calculated values of apparent activation energy, E_a , activation enthalpies, ΔH^\ddagger , and activation entropies, ΔS^\ddagger are given in Table 5 and Table 6. These values indicate that the presence of inhibitor decreases the activation energy, E_a , and the activation enthalpies, ΔH^\ddagger . A decrease in inhibition efficiency with rise in temperature, with analogous increase in corrosion activation energy in the presence of inhibitor compared to its absence, is frequently interpreted as being suggestive of multilayer physical adsorption mechanism. The reverse effect, corresponding to an increase in inhibition efficiency with rise in temperature and lower activation energy in presence of inhibitor, suggests the formation of chemisorbed monolayer [38, 40]. The values of ΔS^\ddagger are lower for inhibited solutions than that for the uninhibited solutions. The lower values of ΔS^\ddagger in the presence of the inhibitors implies that the activated complex is the rate determining step and represents association rather than dissociation meaning that a decrease in disordering taking place on going from reactants to the activated complex [41]. Thus, the entropy of the associated activated complex is lower compared to the reactants. This refers to the formation of activated complex from the reactants but not metal adsorbed- species reaction complex from reactants.

3.5. Adsorption isotherm

In order to understand the mechanism of corrosion inhibition, the adsorption behavior of the organic adsorbate on the aluminum surface must be known. The degree of surface coverage (θ) for different concentration of inhibitor was evaluated from potentiodynamic polarization measurements. A correlation between θ and inhibitor concentration in the corrosive

medium can be represented by the Langmuir adsorption isotherm.

$$\frac{\theta}{(1-\theta)} = K_{\text{ads}} C \quad (11)$$

where K_{ads} is the equilibrium constant of the inhibitor adsorption process and C is the inhibitor concentration.

A straight line was obtained on plotting C/θ against C , suggesting that the adsorption of the compound on aluminum surface follows Langmuir adsorption isotherm model. The slopes are close to 1, and the strong correlation ($R^2 > 0.99$) proved that the adsorption of EAMT on the metal surface obeyed to the Langmuir's adsorption isotherm. They might be the results of the interactions between the adsorbed species on the metal surface [43]. The high values of K for the studied inhibitor indicate strong adsorption of inhibitor on the alloy surface. Adsorption isotherm for different concentrations of EAMT, on the surface of 6061 Al- SiC composite and base alloy in 0.5 M sulphuric acid at different temperatures are shown in Fig. 14 and Fig. 15.

The free energy of adsorption, ΔG_{ads}^0 was calculated using the relation,

$$\Delta G^0 = -RT \ln \left[\frac{\theta}{C(1-\theta)} \right] \quad (12)$$

where C is the concentration of the inhibitor expressed in mole dm^{-3} . The calculated values of ΔG_{ads}^0 for EAMT on the composite and the base alloy were in the range of -27.3 to -33.7 kJ mol^{-1} and -27.9 to 34.6 kJ mol^{-1} , respectively. The negative values of ΔG_{ads}^0 suggest the spontaneous adsorption of EAMT on the composite and base alloy surfaces. Since the values of ΔG_{ads}^0 of -40 kJ mol^{-1} is usually accepted as threshold value between chemisorption and physisorption, the obtained values of the ΔG_{ads}^0 may be indicative of both physical and chemical process [44]. According to Fragnani and Trabaneli [45], sulfur-containing substances easily chemisorb onto the surface of metal in acid media, whereas nitrogen containing compounds tend to favor physisorption. This suggestion has been corroborated by the results of other authors [46].

The enthalpy of adsorption was calculated using rearranged form of Gibbs – Helmholtz equation

$$\Delta G_{\text{ads}}^0 = \Delta H_{\text{ads}}^0 - T \Delta S_{\text{ads}}^0 \quad (13)$$

The variation of ΔG_{ads}^0 with T for both the composite and base alloy gives straight line with intercept that equals ΔH_{ads}^0 (Fig. 16 and Fig. 17). Figure shows the good dependence of ΔG_{ads}^0 on T , indicating good correlation among thermodynamic parameters. The thermodynamic data obtained for EAMT adsorbed on aluminum composite and base alloy are depicted in Table 7. The positive sign of ΔH_{ads}^0 in sulphuric acid solution indicates that the adsorption of inhibitor molecule is an endothermic process. Generally, an exothermic adsorption process ($\Delta H_{\text{ads}}^0 < 0$) signifies

either physisorption or chemisorptions, while endothermic process ($\Delta H_{\text{ads}}^0 > 0$) is attributable to chemisorption [47]. In the present work, the absolute values of ΔH_{ads}^0 for the adsorption of EAMT in 0.5 M H_2SO_4 is $31.84 \text{ kJ mol}^{-1}$ and $35.97 \text{ kJ mol}^{-1}$ for the composite and base alloy respectively, indicating that this inhibitor is chemically adsorbed. The ΔS_{ads}^0 values in the presence of inhibitor are positive, meaning a increase in disordering on going from reactants to metal adsorbed species [48]. The increase in disordering may be due to desorption of already adsorbed water molecules on the aluminium surface. This may overweigh the ordering of complex molecules resulting from the adsorption of only inhibitor. The observed disordering may also be due to the complexity of chemisorption involved on the surface of the metal [49].

3.6. Effects of acid concentration

It was observed that as concentration of the acid media increases, the inhibition efficiency also increases. The order of increase of inhibition efficiency in different acid media is as follows. $0.5 \text{ M} > 0.25 \text{ M} > 0.125 \text{ M}$.

The explanation for the above trend are based on the behaviour of anions in the aggressive acid media. Prabhu *et al.* [42] have explained the interference of the added inhibitor in the dissolution reaction at the metal surface in two different ways i) competitive and ii) co-operative adsorption processes. In the first way, the inhibitor containing heterocyclic chemisorption centres like N, O and S competes with anions of the acid media like SO_4^{2-} for sites at the water covered anodic surface. In doing so, the protonated inhibitor loses its associated protons to water molecules and enters the double layer and chemisorbs by donating electrons to the metal. In the second way, the protonated inhibitor electrostatically adsorbs onto the anion covered surface, through its cationic form. The adsorption mechanism may occur as follows.

- Firstly, the acid's anions (SO_4^{2-}) adsorb physically on the positively charged metal surface, giving rise for a net negative charge on the metal surface.
 - Secondly, the organic cations are physically attracted to the anions layer which is formed on the metal surface.
- Both these factors facilitates the higher adsorption of inhibitor in higher concentrated acid medium. In the present study, the mechanism of inhibition of EAMT in all the three acid media takes place in both ways but predominantly according to the first way.

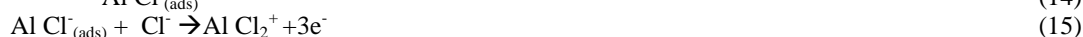
As observed from the Table 7, the corrosion rate as well as the inhibition efficiency increases with increase in sulphuric acid concentration and is maximum in 0.5 M solution. The increase in the extent of adsorption of the inhibitor on the alloy surface and in turn the increase in the inhibition efficiency can be attributed to the following two facts:

The increase in the concentration of the acid increases the extent of protonation of the inhibitor molecules, thereby facilitating their adsorption on the cathodic sites.

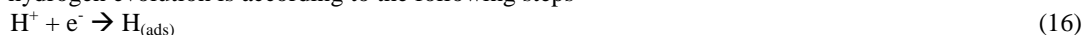
With the increase in the concentration of the acid, the anion of the acid (SO_4^{2-}) adsorb physically on the positively charged metal surface, giving rise to a net negative charge on the metal surface [34]. This further facilitates the adsorption of protonated inhibitor molecules.

3.7. Mechanism of inhibition

The corrosion inhibition property of EAMT through adsorption on the surface of the composite or the base alloy can be attributed to the presence of electronegative elements like nitrogen and sulphur and also to the presence of π electrons on the benzene ring. The metal surface in contact with a solution is charged due to the electric field that emerges at the interface on the immersion in the electrolyte. This can be determined, according to Antrapov *et al.* [50] by comparing the zero charge potential and the rest potential of the metal in the corresponding medium. The value of pH_{Zch} , which is defined as the pH at a point of zero charge is equal to 9.1 for aluminum [51]. So aluminum is positively charged in highly acidic medium, as the ones used in this investigation. Therefore, sulphate ions and EAMT can be adsorbed on aluminium surface via their negative centres. Also, EAMT can be protonated in the highly acidic solution used in the investigation. The mechanism of adsorption of protonated EAMT can be predicted on the basis of the mechanism proposed for the corrosion of aluminum in hydrochloric acid [52]. According to this mechanism, anodic dissolution of Al follows steps



The cathodic hydrogen evolution is according to the following steps



In acidic solution, the nitrogen atom of the amino group can be protonated. The protonated molecules can adsorb on the cathodic sites of aluminum in competition with the hydrogen ions (equation 16). Co-ordinate covalent bond formation between electron pairs of unprotonated S atom and metal surface can take place. Further, EAMT molecules are chemically adsorbed due to interaction of π -orbitals with metal surface following deprotonisation step of the physically adsorbed protonated molecules. In the present case, the value of ΔG_{ads}^0 is $-27.33 \text{ kJ mol}^{-1}$ to $-34.63 \text{ kJ mol}^{-1}$, hence indicated that adsorption of EAMT on the surface of aluminum involves both physical and chemical process. But, as it can be seen from Table 7, the values of ΔG_{ads}^0 increased with increasing temperature, indicating that EAMT adsorbed chemically on the surface of aluminum composite and base alloy.

3.8. Scanning electron microscopy

In order to evaluate the effect of corrosion on the surface morphology of the composite and the base alloy, SEM analysis was carried out on the samples subjected to corrosion in acid mixture containing 0.5 M sulphuric acid in the presence and absence of the inhibitors. The SEM images of freshly polished surface of the composite are given in Fig. 18. Fig.19 shows deep cavities formed due to detachment of SiC particle from the composite when exposed to the acid mixture medium. This may be attributed to the corrosion at the interface between the particle and matrix due to the galvanic action, with the particle acting as a cathodic site and resulting in the detachment of the particle from the matrix. Fig. 20 show more or less smooth surfaces of the composite, without pits in the presence of inhibitors. It can be concluded that, the adsorbed layer of inhibitor provides a corrosion free smooth surface on the composite

In order to gain the information about the surface composition of the composite and base alloy, EDX studies were carried out on samples which were exposed to the corrosion medium in the presence and absence of the inhibitor. EDX spectra of the composite sample exposed to the sulphuric acid medium in the absence of inhibitor showed spectral lines corresponding to aluminium, silicon, oxygen and negligibly small peak corresponding to sulphur of sulphate. In the spectra of the base alloy, the sulphur peaks were not at all visible. The composite exposed to corrosion medium in the presence of inhibitors showed additional carbon and nitrogen signals, indicating surface coverage by the inhibitor. Presence of higher percentage of carbon and nitrogen on the surface of the composite samples than on base alloy reveals the higher adsorption of EAMT on the composite than on the base alloy. This also accounts for higher inhibition efficiency achieved on composite sample than on the base alloy sample.

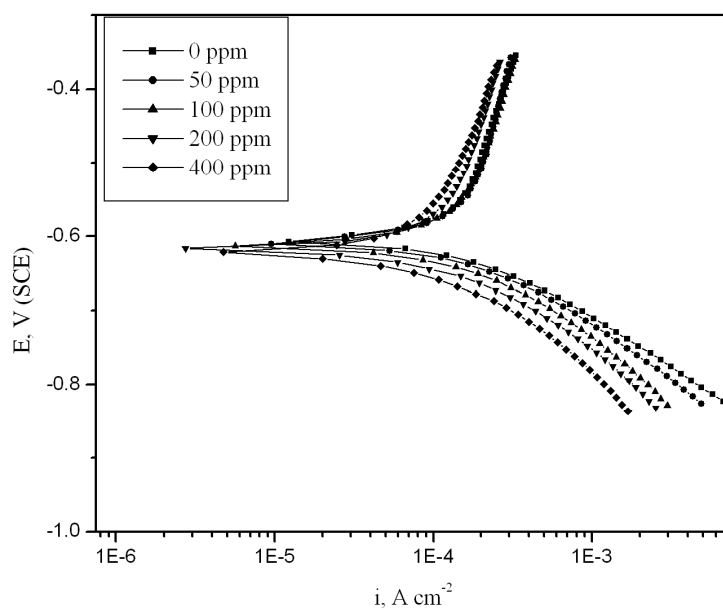


Fig. 1. Polarisation curves of 6061 Al- SiC composite in 0.5 M H_2SO_4 at 30 °C in presence of different concentrations of EAMT

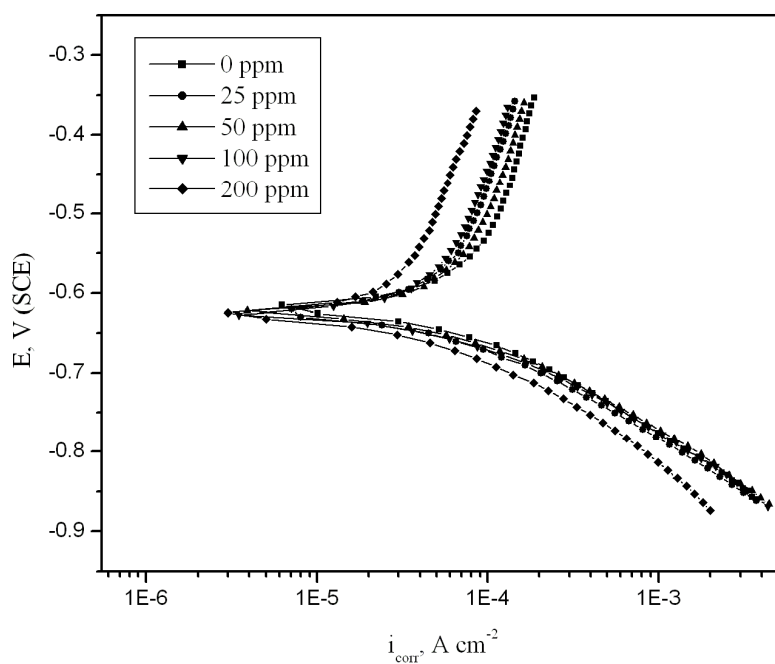


Fig. 2. Polarization curves of 6061 base alloy in 0.5 M H_2SO_4 at 30 °C in presence of different concentrations of EAMT

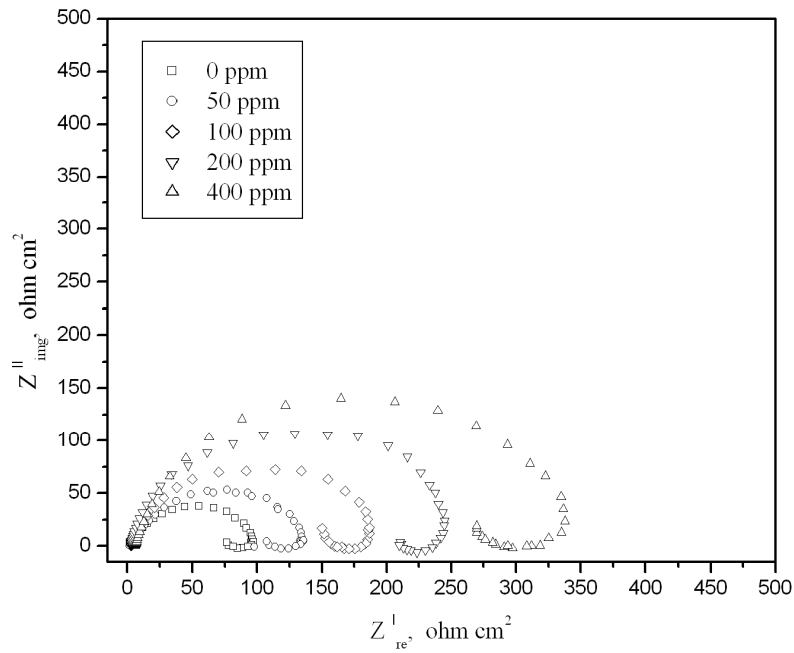


Fig. 3. Nyquist plots of 6061 Al- SiC composite in 0.5 M H₂SO₄ at 30 °C in presence of different concentrations of EAMT

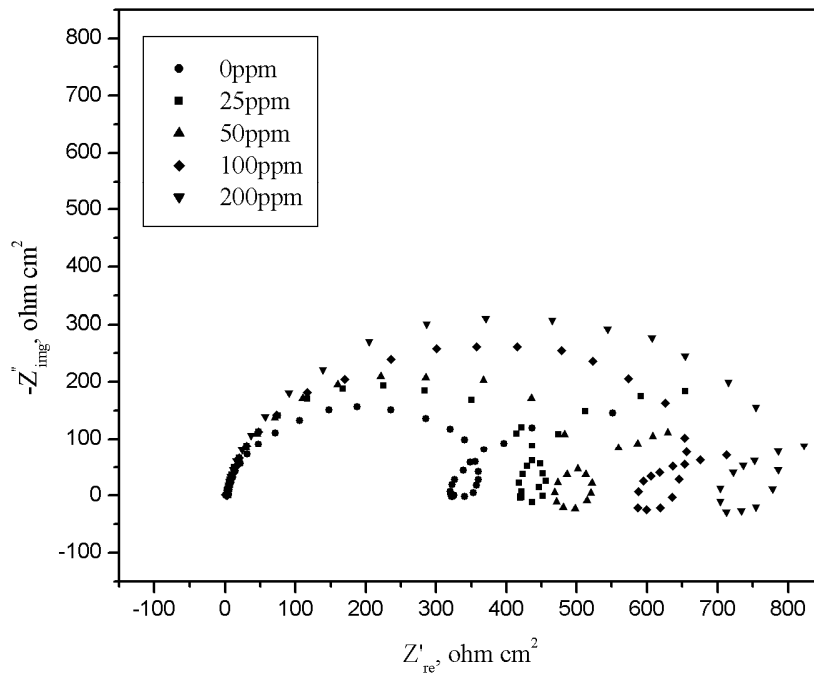


Fig. 4. Nyquist plots of 6061 base alloy in 0.5 M H₂SO₄ at 30 °C in presence of different concentrations of EAMT

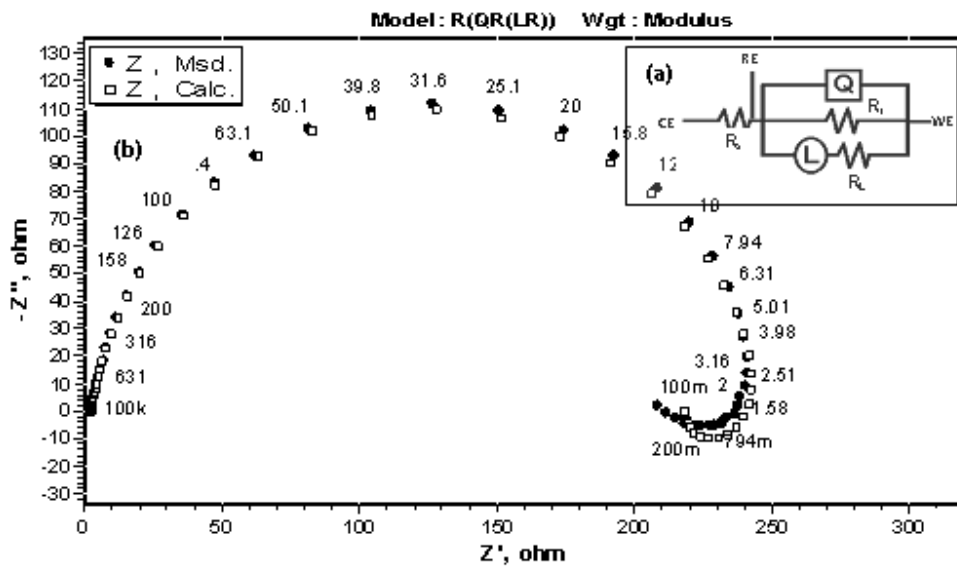


Fig. 5. The equivalent circuit model used to fit the experimental data of the composite

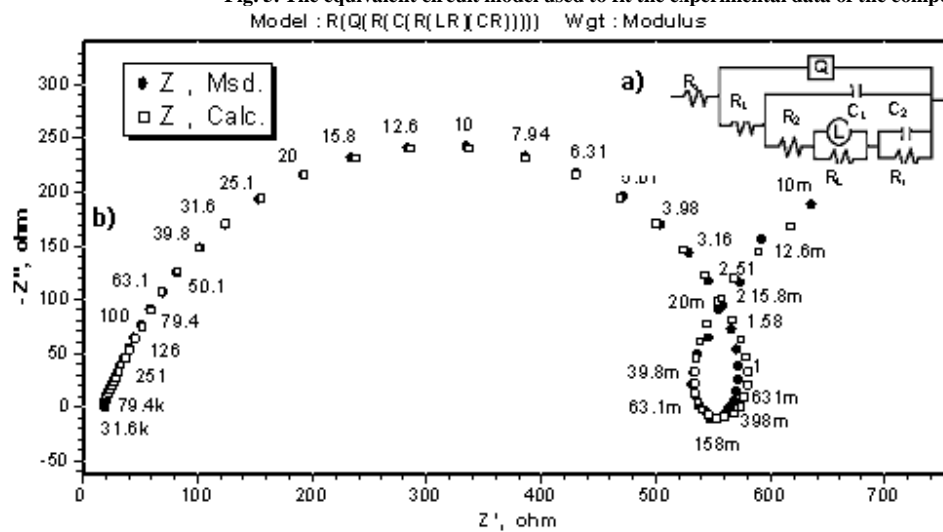


Fig. 6. The equivalent circuit model used to fit the experimental data of the base alloy

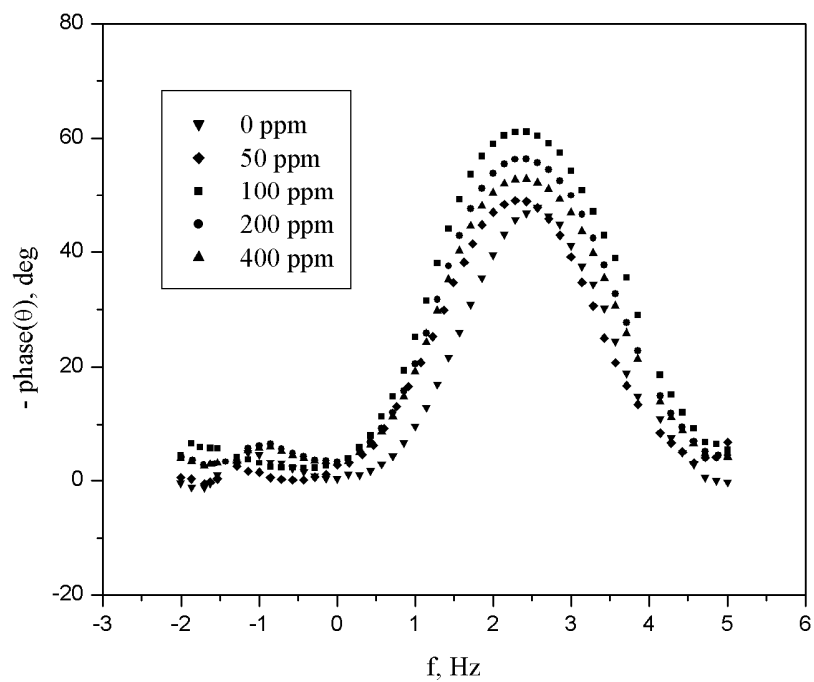


Fig. 7. Bode plots of 6061 composite in 0.5 M H_2SO_4 at 30 °C in presence of different concentrations of EAMT

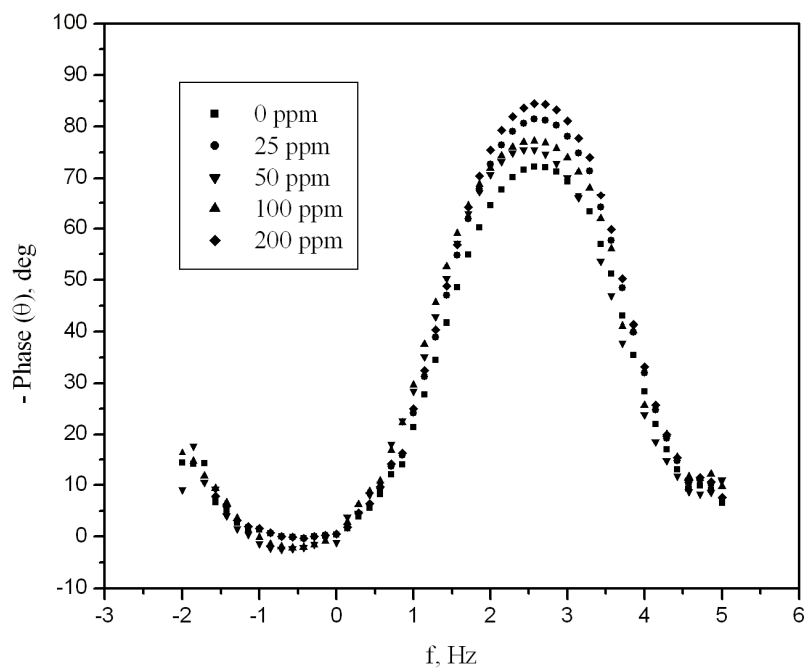


Fig. 8. Bode plots of 6061 base alloy in 0.5 M H_2SO_4 at 30 °C in presence of different concentrations of EAMT

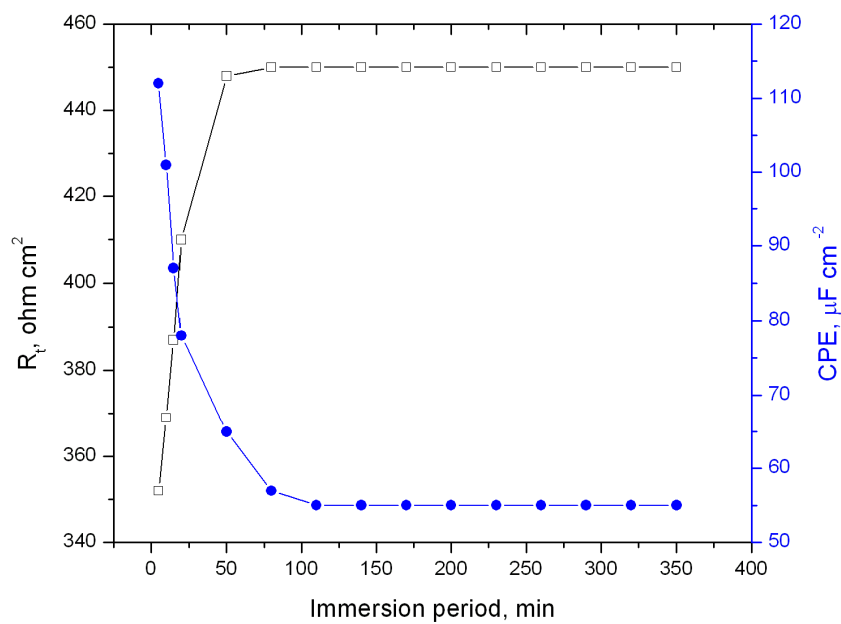


Fig. 9. Dependence of both R_t and CPE on the immersion time for Al composite in 0.5 M sulphuric acid solution

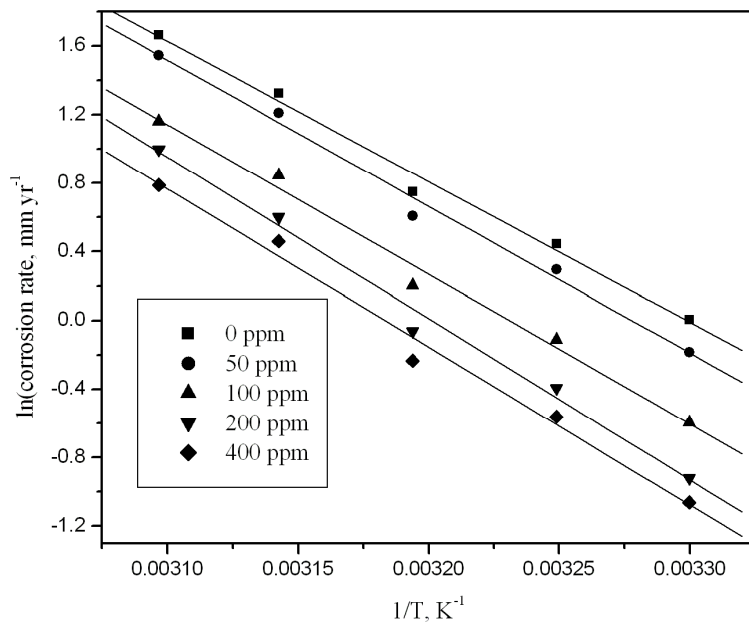


Fig.10. Arrhenius plots for the composite in 0.5 M H_2SO_4 at different concentrations of EAMT

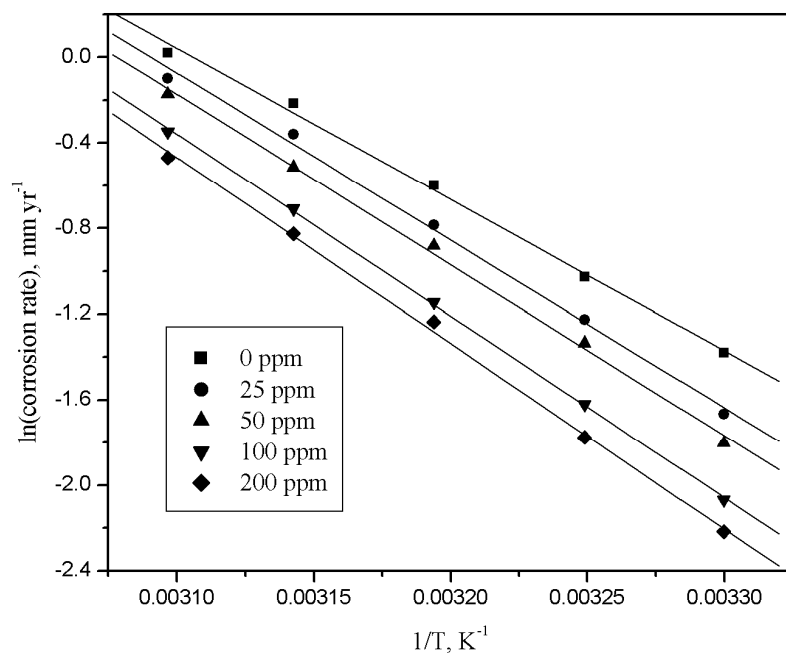


Fig.11. Arrhenius plots for the base alloy in 0.5 M H₂SO₄ at different concentrations of EAMT

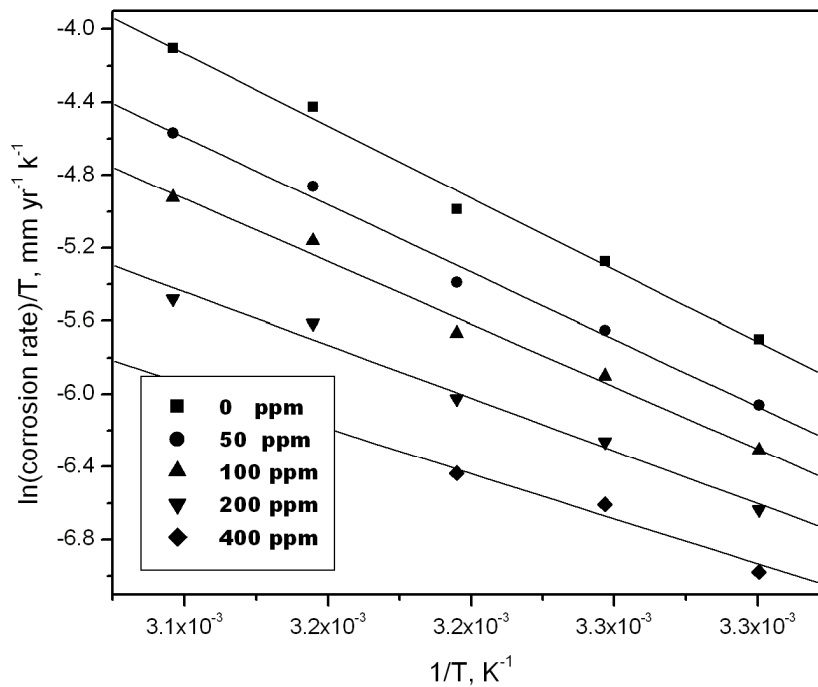


Fig.12. ln(corrosion rate)/T vs 1/T for composite in 0.5 M H₂SO₄ at different concentrations of EAMT

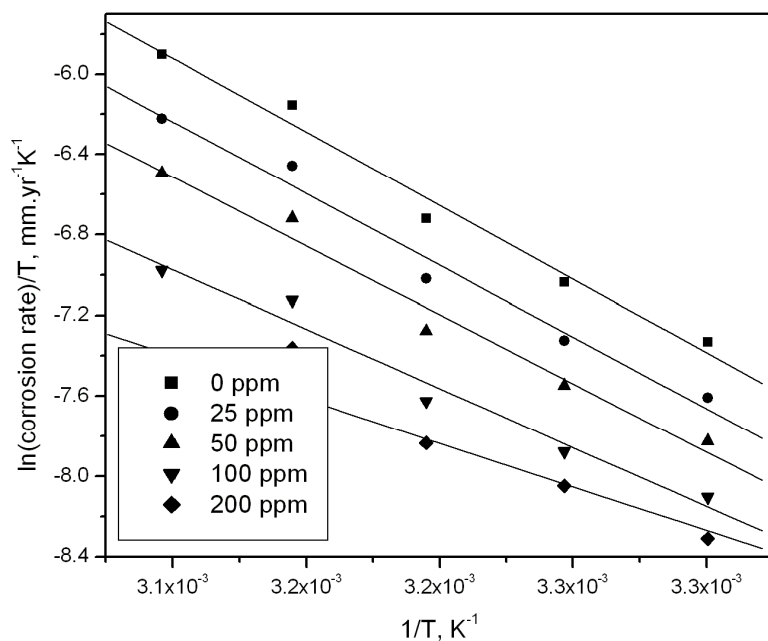


Fig.13. $\ln(\text{corrosion rate}/T)$ vs $1/T$ for base alloy in 0.5 M H_2SO_4 at different concentrations of EAMT

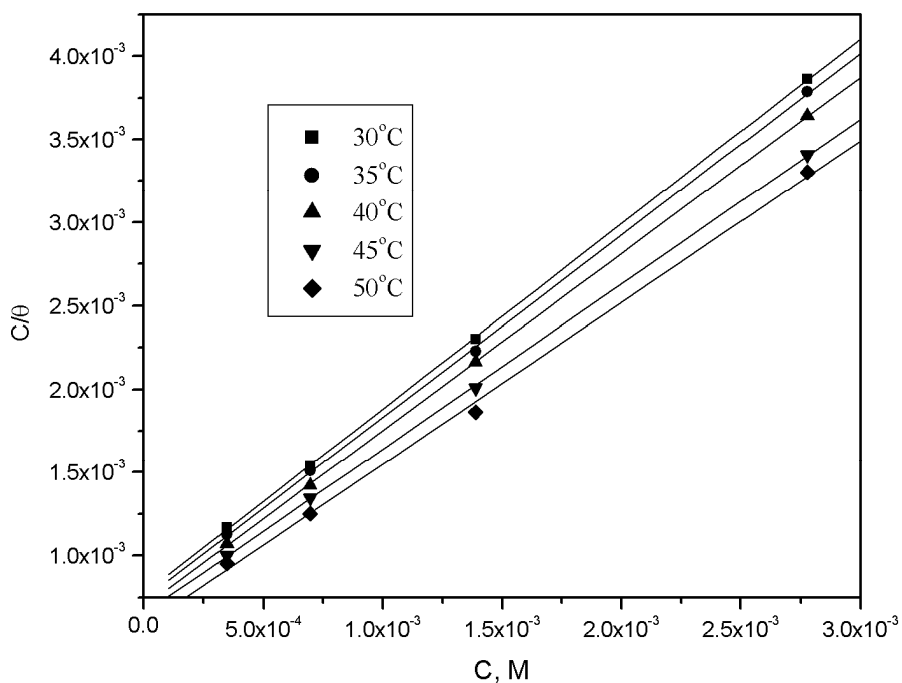


Fig.14. Curve fitting of corrosion data for the composite in 0.5 M H_2SO_4 in presence of different concentrations of the EAMT to Langmuir adsorption isotherm at 30 °C – 50 °C

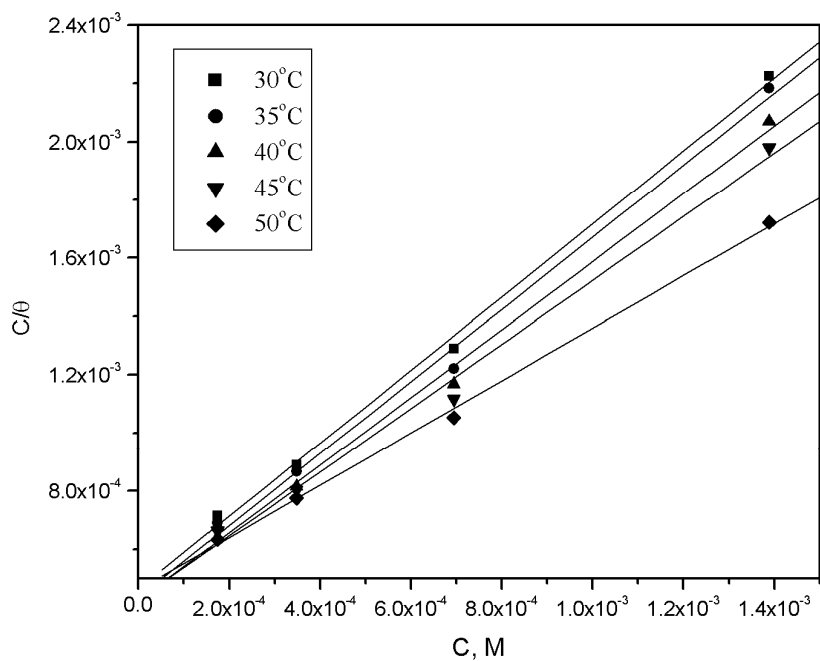


Fig.15. Curve fitting of corrosion data for the base alloy in 0.5 M H₂SO₄ in presence of different concentrations of the EAMT to Langmuir adsorption isotherm at 30 °C – 50 °C

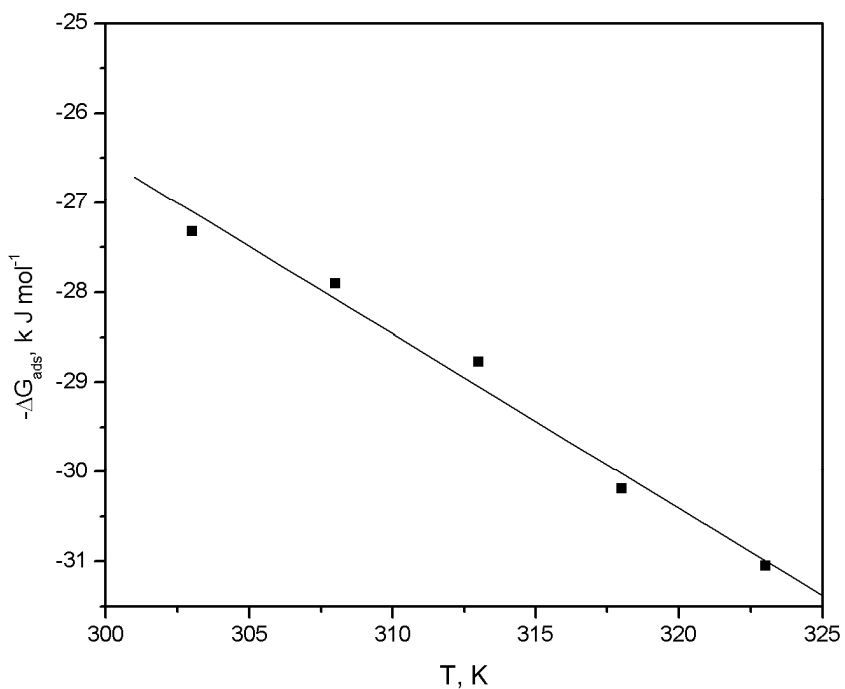


Fig.16. Adsorption isotherm plot for ΔG^0 vs. T for the composite

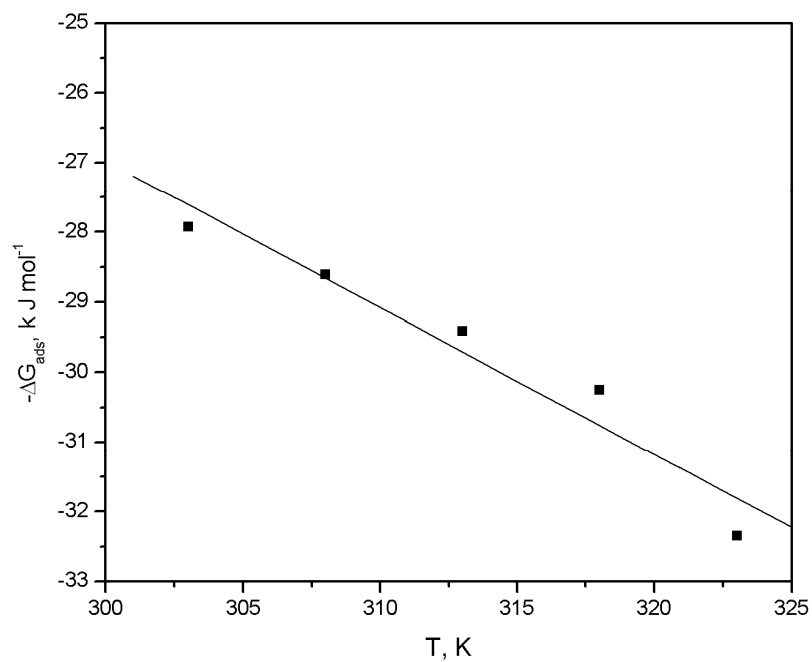


Fig.17. Adsorption isotherm plot for ΔG^0 vs. T for the base alloy

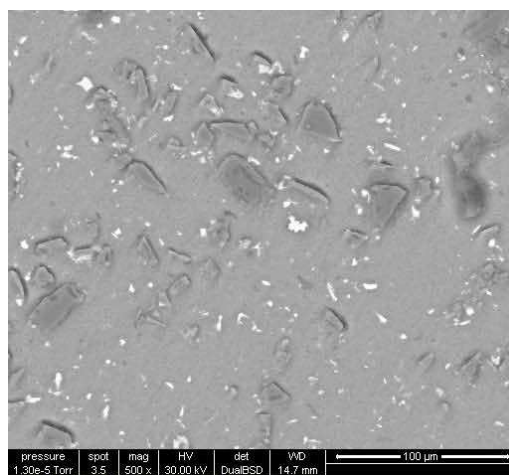


Fig.18. SEM image of the freshly polished surface of the composite

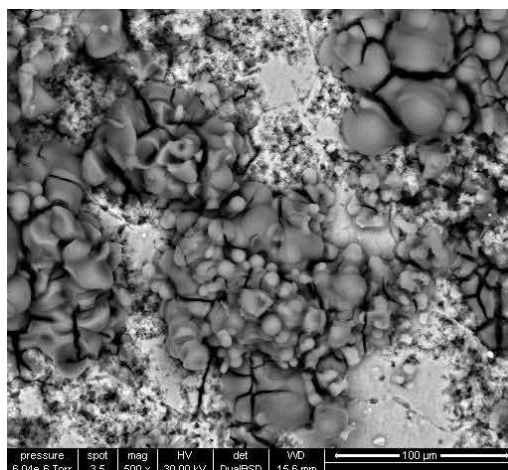


Fig.19. SEM image of the surface of composite immersed for 168 hr in 0.5 M H₂SO₄ in the absence of EAMT

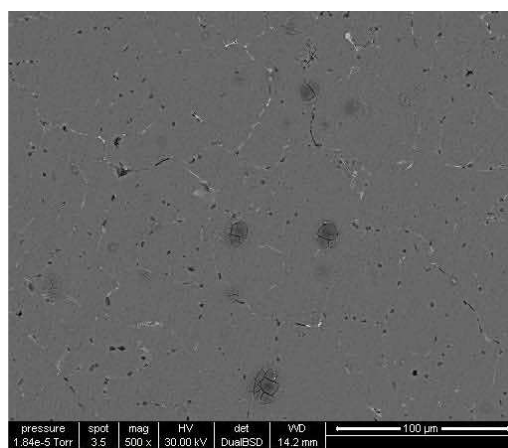


Fig. 20. SEM image of the surface of composite immersed for 168 hr in 0.5 M H₂SO₄ in the presence of 400 ppm of EAMT

Table 1 The composition of the base metal Al 6061 alloy

Element	Cu	Si	Mg	Cr	Al
Composition (Wt.%)	0.25	0.6	1.00	0.25	Bal

Table 2 Electrochemical parameters obtained from potentiodynamic polarisation measurements of Al composite and its base alloy at various concentrations of EAMT at 30 °C

Composite						Base alloy				
Conc of the medium M	Conc. of inhibitor (ppm)	E_{corr} (mV) (SCE)	i_{corr} ($\mu A cm^{-2}$)	$-b_c$ (mVdec ⁻¹)	IE %	Conc. of inhibitor (ppm)	E_{corr} (mV) (SCE)	i_{corr} ($\mu A cm^{-2}$)	$-b_c$ (mVdec ⁻¹)	IE %
0.5	0	-599	91.4	59		0	-605	18.05	35	
	50	-611	64.3	56	29.6	25	-612	13.67	30	24.3
	100	-613	50.1	52	45.2	50	-614	11.00	29	39.0
	200	-617	36.2	53	60.4	100	-618	8.33	28	53.8
	400	-620	25.7	50	71.9	200	-624	6.78	25	62.4
0.25	0	-615	44.8	56		0	-622	10.45	28	
	25	-632	30.3	55	32.4	10	-635	8.56	24	18.1
	50	-642	24.4	54	45.5	25	-638	7.17	22	31.4
	100	-646	18.2	50	59.3	50	-634	5.86	21	43.9
	200	-657	13.4	45	70.1	100	-628	5.05	18	51.7
0.125	0	-664	25.50	50		0	-679	5.36	20	
	10	-669	20.20	45	20.8	5	-682	4.68	15	12.7
	25	-681	15.91	43	37.6	10	-689	4.23	13	21.1
	50	-687	13.29	42	47.8	25	-694	3.75	12	30.0
	100	-691	10.10	40	60.4	50	-706	3.11	10	42.0

Table 3 Electrochemical parameters obtained from EIS measurements of Al composite and its base alloy at various concentrations of EAMT at 30 °C

Composite					Base alloy				
Conc. of the medium (M)	Conc. of inhibitor (ppm)	R_p (Ωcm^2)	CPE ($\mu F cm^{-2}$)	IE (%)	Conc. of inhibitor (ppm)	R_p (Ωcm^2)	CPE ($\mu F cm^{-2}$)	IE (%)	
0.5	0	93.9	222		0	360	27.1		
	50	136	182	30.5	25	483	26.6	25.3	
	100	176	155	46.7	50	608	25.2	40.2	
	200	245	135	61.3	100	809	23.2	55.6	
	400	345	122	72.5	200	956	19.5	62.9	
0.25	0	268	179		0	457	23.4		
	25	403	142	33.4	10	567	21.8	19.1	
	50	501	136	46.8	25	678	18.4	32.6	
	100	684	122	60.3	50	832	16.6	45.3	
	200	998	113	71.2	100	986	12.3	53.8	
0.125	0	521	101		0	720	14.4		
	10	660	92.2	21.8	5	830	8.32	13.6	
	25	843	86.3	38.1	10	923	5.84	22.0	
	50	1012	77.6	48.3	25	1083	4.75	33.4	
	100	1356	56.4	61.2	50	1256	2.91	42.8	

Table 4 Electrochemical parameters obtained from PDP measurements of Al composite and its base alloy in 0.5 M H₂SO₄ in absence and presence of various concentrations of EAMT

Temp. of medium (°C)	Conc. of inhibitor (ppm)	Composite				Base alloy				
		E _{corr} (mV (SCE))	i _{corr} (μA cm ⁻²)	-b _c (mVdec ⁻¹)	IE (%)	E _{corr} (mV (SCE))	i _{corr} (μA cm ⁻²)	-b _c (mVdec ⁻¹)	IE (%)	
30	0	-599	91.4	59		0	-605	18.05	35	
	50	-611	64.3	56	29.6	25	-612	13.67	30	24.3
	100	-613	50.1	52	45.2	50	-614	11	29	39.0
	200	-617	36.2	53	60.4	100	-618	8.33	28	53.8
	400	-620	25.7	50	71.9	200	-624	6.78	25	62.4
35	0	-608	142	61		0	-615	24.63	39	
	50	-615	98.3	59	30.8	25	-618	18.43	36	25.2
	100	-620	76.6	58	46.0	50	-620	14.75	33	40.1
	200	-621	53.4	55	62.4	100	-623	10.62	31	56.9
	400	-623	37.8	53	73.4	200	-627	8.96	28	63.6
40	0	-615	192.5	65		0	-627	34.27	48	
	50	-620	130	60	32.5	25	-629	25.46	43	25.7
	100	-624	98.4	58	48.9	50	-630	19.65	40	42.7
	200	-627	68.9	54	64.2	100	-635	13.89	39	59.5
	400	-631	45.6	50	76.3	200	-636	11.27	37	67.1
45	0	-632	342.3	69		0	-640	61.45	50	
	50	-634	223.4	65	34.7	25	-644	45.35	48	26.2
	100	-642	165.6	64	51.6	50	-647	34.86	41	43.3
	200	-643	105.7	60	69.1	100	-651	23.26	35	62.1
	400	-646	63.2	57	81.5	200	-653	18.34	33	70.1
50	0	-646	480.1	70		0	-653	80.4	52	
	50	-649	305.1	62	36.4	25	-655	58.34	54	27.4
	100	-659	213.4	60	55.5	50	-656	44.39	47	44.8
	200	-662	122.5	58	74.5	100	-661	27.38	44	65.9
	400	-667	76.3	56	84.1	200	-662	19.84	45	75.3

Table 5 Activation parameters of the corrosion of 6061 Al-SiC composite in absence and presence of different concentrations of EAMT

Activation parameters	Concentration of the medium in M														
	0.5 M H ₂ SO ₄					0.25 M H ₂ SO ₄					0.125 M H ₂ SO ₄				
	Inhibitor concentration (ppm)					Inhibitor concentration (ppm)					Inhibitor concentration (ppm)				
	0	50	100	200	400	0	25	50	100	200	0	10	25	50	100
E _a (kJ mol ⁻¹)	68.3	64.0	59.7	50.9	43.8	71.7	67.7	65.9	58.9	51.7	82.4	75.6	71.8	68.7	65.7
ΔH [#] (kJ mol ⁻¹)	65.6	61.4	57.1	48.3	41.2	69.1	65.1	63.3	56.3	41.1	79.4	73.0	69.2	66.1	63.1
-ΔS [#] (J K ⁻¹ mol ⁻¹)	23.3	45.7	61.5	93.9	119.7	24.1	33.5	48.2	73.3	99.5	5.8	49.9	64.0	75.7	88.1

Table 6 Activation parameters of the corrosion of 6061 Al base alloy in absence and presence of different concentrations of EAMT

Activation parameters	Concentration of the medium in M														
	0.5 M H ₂ SO ₄					0.25 M H ₂ SO ₄					0.125 M H ₂ SO ₄				
	Inhibitor concentration (ppm)					Inhibitor concentration (ppm)					Inhibitor concentration (ppm)				
	0	25	50	100	200	0	10	25	50	100	0	5	10	25	50
E _a (kJ mol ⁻¹)	63.4	61.8	59.3	51.4	38.8	69.2	63.7	61.9	58.9	55.8	78.9	75.4	73.9	70.1	65.7
ΔH [#] (kJ mol ⁻¹)	60.8	59.2	56.7	48.8	36.2	66.6	61.1	59.3	56.3	53.1	76.4	72.8	71.3	67.5	63.1
-ΔS [#] (J K ⁻¹ mol ⁻¹)	58.2	66.5	76.5	135.5	147.2	44.0	64.0	71.5	83.1	93.9	16.6	29.9	36.6	49.1	64.8

Table 7 Inhibition efficiencies of composite and base alloy in various concentrations of sulphuric acid at 50 °C.

Conc. of the medium (M)	Composite			Base alloy		
	Optimum inhibitor concentration (ppm)	Inhibition efficiency (IE %)		Optimum inhibitor concentration (ppm)	Inhibition efficiency (IE %)	
		Tafel method	EIS method		Tafel method	EIS method
0.5	400	84.1	85.2	200	75.2	77.0
0.25	200	82.3	83.6	100	65.2	66.9
0.125	100	71.1	71.6	50	58.4	60.1

Table 8 Thermodynamic parameters for the adsorption of EAMT on Al composite and base alloy in a mixture of 0.5 M sulphuric acid at different temperatures

Temperature (°C)	Composite				Base alloy			
	K M ⁻¹	ΔG_{ads}^0 (kJ mol ⁻¹)	ΔH_{ads}^0 ((kJ mol ⁻¹)	ΔS_{ads}^0 (J mol ⁻¹ K ⁻¹)	K M ⁻¹	ΔG_{ads}^0 (kJ mol ⁻¹)	ΔH_{ads}^0 ((kJ mol ⁻¹)	ΔS_{ads}^0 (J mol ⁻¹ K ⁻¹)
30	1295.3	-26.57	31.84	194	2155.2	-27.28	35.97	209
35	1351.4	-26.77	31.84	194	2298.9	-27.42	35.97	209
40	1443.0	-27.11	31.84	194	2358.5	-27.70	35.97	209
45	1538.5	-27.02	31.84	194	2341.9	-27.73	35.97	209
50	1730.1	-27.26	31.84	194	2173.9	-28.01	35.97	209

CONCLUSION

1. EAMT acts as a good corrosion inhibitor for 6061 Al- 15 vol. pct. SiC_(p) composite and its base alloy in sulphuric acid medium.
2. Corrosion inhibition efficiency of EAMT increases with increasing concentration of inhibitor up to critical concentration.
3. EAMT behaves as cathodic type inhibitor.
4. Inhibition efficiency of EAMT on aluminum composite is more than that of its base alloy.
5. Inhibition efficiency of EAMT on aluminum composite and its base alloy increases with increase in concentration of sulphuric acid and with increase in temperature from 30 °C - 50 °C.
6. Inhibitor obeys Langmuir's model of adsorption and the adsorption is predominantly through chemisorption.
7. The negative value of ΔG_{ads}^0 obtained indicates that EAMT adsorbed spontaneously on both the composite and base alloy. The adsorption process is endothermic with positive value of entropy.
8. SEM and EDX images revealed protection of alloy surface in sulphuric acid medium by the adsorption of EAMT.
9. The inhibition efficiency obtained from potentiodynamic polarization and electrochemical impedance spectroscopy techniques are in good agreement.

REFERENCES

- [1] TH Sanders Jr., EA Starke Jr., Proceedings of the Fifth International Conference on Al-Lithium alloys, Materials & Composites Engineering Publications Ltd., Birmingham, UK, **1989**, 1-40.
- [2] C Monticelli; F Zucchi; G Brunoro; G Trabaneli, *J. Appl. Electrochem.*, **1997**, 27 (3), 325.
- [3] A Pardo; MC Merino; S Merino; F Viejo; M Carboneras; R Arrabal, *Corros. Sci.*, **2005**, 47(7), 1750.
- [4] CE Da Costa; F Velasco; JM Toralba, *Rev. Metal. Madrid*. **2000**, 36(1), 179.
- [5] PK Rohatgi, *JOM*. **1991**, 43(4) 10.
- [6] CJ Peel, R Moreton, PJ Gregson, EP Hunt, Proceedings of the XIII, International Conference on Society of Advanced Material and Process Engineering, SAMPE, Covina, CA, **1991**, 189-197.
- [7] IM Hutchings, S Wilson, AT Alpas, TW Clyne (ed.), *Comprehensive Composite Materials*, Vol.3, Elsevier Science Ltd., UK, **2000**.
- [8] DM Aylor, Corrosion of Metal Matrix Composites, Metals Hand Book, Vol.13, Ninth Edition, ASM, **1987**.
- [9] AJ Trowsdate; B Noble; SJ Haris; ISR Gibbins; GE Thomson; GC Wood, *Corros. Sci.*, **1996**, 38(2), 177-191.
- [10] F Bentiss; Treisnel, M Lagrence, *Br. Corros. J.*, **2000**, 35(2), 315-323.
- [11] AR Suma; Padmalatha; J Nayak; AN Shetty, *J. Met. Mater. Sci.*, **2005**, 47(1), 51-57.
- [12] MN Desai; SM Desai; MH Gandhi; CB Snaha, *Anti-Corros methods mater.*, **1971**, 18(5) 8-12.
- [13] MN Desai; SS. Rana, MH Gandhi, *Anticorros Methods and Mater.*, **1971**, 18(2) 19-21.
- [14] IN Putilova, SA Balezin, B, Arannik, *Metallic Corrosion Inhibitors*, Pergamon, Oxford, **1960**, 67.

- [15] G Trabanelli, V Carassiti, *Advances in Corrosion Science and Technology*, 1, Plenum Press, New York, **1970**, 147.
- [16] IL Rozerfeld, *Corrosion Inhibitors*, McGraw Hill, New York, **1981**, 147-158.
- [17] CC Nathan, *Corrosion Inhibitors*, NACE, Houston, **1973**, 7-15.
- [18] F Hunkeler, H Bohni, *Mater. Corros.*, **1983**, 34, 68-76.
- [19] PT Shah, TC Daniels, *Rev. Trav. Chim.*, **1950**, 69, 1545-1560.
- [20] M Bethencourt, FJ Botana, MA Cauqui, M Marcos, MA, Rodriguez, *J. Alloy Compd.*, **1997**, 250 (1-2), 455.
- [21] SS Abdel Rahim; HH Hassan; MA Amin, *Mater. Chem. Phys.*; **2002**, 78, 337-348.
- [22] K Aramaki, *Corros. Sci.*, **2001**, 43(10), 1985-2000.
- [23] MS Abdl Aal; S Radwan; AE Saied, *Br. Corros.*, **J. 1983**, 18, 102.
- [24] KF Khaled; MM. Al-Qahtani, *Mater. Chem. Phys.*, **2009**, 113, 150.
- [25] S Sayed; Abdel Rehim; H Hamdi Hassan, A Mohammed Amin, *Appl. Surf. Sci.* **2002**, 187(3-4), 279-290
- [26] HJW Lenderink; MVD Linden; JHW De Wit, *Electrochim. Acta*, **1989**, 38(14), 1993.
- [27] JH Wit; HJW Lenderink, *Electrochim. Acta*, **1996**, 41(7-8), 1111.
- [28] JB Bessone; DR Salinas; C Mayer; M Ebert; WJ Lorenz, *Electrochim. Acta*, **1992**, 37(9), 2283.
- [29] SE Frers; MM Stefanel; C Mayer; T Chierchie; *J. Appl. Electrochem.*, **1990**, 20(9), 996-999.
- [30] M Metikos-Hukovic; R Babic, Z Grubac, *J. Appl. Electrochem.*, **1998**, 28(4), 433-439.
- [31] CMA Brett, *J. Appl. Electrochem.*, **1990**, 20, 1000.
- [32] EJ Lee; Pyun, *Corros. Sci.*, **1995**, 37(1), 157-168.
- [33] CMA Brett, *Corros. Sci.*, **1992**, 33(2), 203-210.
- [34] A Ehteram Noor, *Mater. Chem. Phys.*, **2009**, 114 533-541.
- [35] A Aytac; U Ozmen; M Kabasakaloglu, *Mater. Chem. Phys.* **2005**, 89(1), 176-181.
- [36] F Mansfeld; S Lin; K Kim; H Shih, *Corros. Sci.*, **1987**, 27(2), 997-1000.
- [37] F Mansfeld; S Lin; S Kim; H Shih, *Mater. Corros.* **1988**, 39, 487-492.
- [38] MA Migahed, *Mater. Chem. Phys.*, **2005**, 93 48-53.
- [39] ES Ivanov, *Inhibitors for Metal Corrosion in Acid Media*, Metallurgy, Moscow, Russia, **1986**.
- [40] S Martinez; I Stern, *J. Appl. Electrochem. Soc.*, **2001**, 31(9) 973-978.
- [41] M Abdallah, *Corros. Sci.*, **2004**, 46 (8), 1981-1996.
- [42] RA Prabhu; AV Shanbhag; TV Venkatesha, *Bull. Electrochem.*, **2006**, 22(3), 225-231.
- [43] MA Ashish Kumar Singh; MA Quraishi, *Corros. Sci.*, **2010**, 52 (1,) 152-160.
- [44] E Geler; DS Azambuja, *Corros. Sci.*, **2000**, 42(4), 631-643.
- [45] A Fragnani; G Trabanelli, *Corrosion*, **1999**, 55 (1), 653-660.
- [46] GK Gomma; MH Wahdan, *Bull. Chem. Soc. Jpn.*, **1994**, 67(10), 2621-2626.
- [47] W Durnie; R De Marco; B Kinsella ; A Jefferson, *J. Electrochem. Soc.*, **2001**, 31(11), 1221-1226.
- [48] G Banerjee ; SN Malhotra, *Corrosion*, **1992**, 48(1), 10-15.
- [49] F Bentiss; M Lebrini; M. Lagrenee, *Corros. Sci.*, **2005**, 47(12), 2915-2931.
- [50] LI Antropov; EM Makushin; VF Panasenko, *Metallic Corrosion Inhibitors*, Kiev, Technika, **1981** 182.
- [51] M Tschapek; C Wasowski; RM Torres Sanchez, *J. Electroanal. Chem.* **1976**, 74(2), 167-176.
- [52] AA Awady, BA Abd. El- Nabey, SG Aziz, *J. Chem. Soc., Faraday Trans.* **1993**, 84(5) 795-802.